Acceptance Testing of the Advanced Electric Propulsion System Qualification and Flight Thrusters

IEPC-2025-213

Jason D. Frieman[1], George C. Soulas[2], Hani Kamhawi[3], Matthew J. Baird[4], and Rohit Shastry[5]
NASA Glenn Research Center, Cleveland, OH, 44135 USA

Hannah Watts[6], Nicholas A. Branch[7], and Eleanor Forbes[8]
Aerojet Rocketdyne, Redmond, WA, 98052 USA

Abstract: This work presents a summary of the Acceptance Test Program performed on the qualification and flight units of the 12 kW Advanced Electric Propulsion System. This test program is led by Aerojet Rocketdyne and consists of acceptance vibration, acceptance hot fire, and final functional measurements and inspections. As of this work, acceptance testing has been completed on one qualification unit and two flight units. No statistically significant unit-to-unit variation was measured, and all three units successfully completed acceptance testing.

I. Motivation and Background

NASA continues to evolve a human exploration approach for beyond low-Earth orbit in a manner involving international, academic, and industry partners [1]. The center of this approach is NASA's Gateway, which is envisioned to provide a maneuverable outpost in lunar orbit to extend human presence in deep space and expand on NASA's exploration goals. The Gateway represents the initial step in NASA's architecture for sustained human cislunar operations, lunar surface access, and missions to Mars.

NASA announced at the May 2020 NASA Advisory Council's Human Explorations and Operations Committee a plan

[1] Solar Electric Propulsion Flight Test Lead, Electric Propulsion Systems Branch, jason.d.frieman@nasa.gov.
[2] Solar Electric Propulsion Qualification Test Lead, Electric Propulsion Systems Branch, george.c.soulas@nasa.gov
[3] Solar Electric Propulsion Thruster Lead, Electric Propulsion Systems Branch, hani.kamhawi-1@nasa.gov.
[4] Research Engineer, Electric Propulsion Systems Branch, matthew.j.baird@nasa.gov.
[5] Solar Electric Propulsion Product Lead Engineer, Electric Propulsion Systems Branch, rohit.shastry@nasa.gov.
[6] Test Engineer, Electric Thrusters, hannah.watts@l3harris.com.
[7] Senior Engineer, Electric Thrusters, nicholas.branch2@l3harris.com.
[8] Chief Engineer, Advanced Electric Propulsion System, eleanor.forbes@l3harris.com.

that calls for launching the first two elements of Gateway as a co-manifested mission [2]. Launching the Power and Propulsion Element (PPE) and the Habitation and Logistics Outpost together reduces mission risk, utilizes PPE's high-power Solar Electric Propulsion (SEP) system to transport both elements to lunar orbit, and reduces overall cost. NASA and Maxar Technologies have a commercial partnership to develop the high-power SEP spacecraft [3,4]. PPE includes both the 12-kW Advanced Electric Propulsion System (AEPS) - developed by Aerojet Rocketdyne an L3Harris Technologies Company (AR) - and a Maxar-developed 6-kW Hall current thruster (HCT) system for a total beginning of life propulsion power of over 48 kW [5].

The NASA Glenn Research Center (GRC) and the Jet Propulsion Laboratory (JPL) led the development of the 12-kW Hall thruster system beginning with maturation of the Hall Effect Rocket with Magnetic Shielding (HERMeS) Technology Demonstration Units (TDUs). Technology development transitioned to AR in May 2016 via the AEPS contract, which is managed by NASA GRC with funding from NASA's Space Technology Mission Directorate under the Technology Demonstration Missions Program and the Exploration Systems Development Mission Directorate via PPE [6].

Under the AEPS contract, AR designed and built a pair of Engineering Test Unit (ETU) thrusters that were derived from the HERMeS TDUs but included modifications to improve manufacturability and ease spacecraft integration [6]. These ETU thrusters, as well as several individual thruster components, underwent a detailed development test campaign that encompassed all test phases planned for qualification including detailed performance assessments, wear tests, and environmental testing (i.e., vibration, shock, and thermal vacuum) [6–8]. Between testing of the HERMeS TDUs and AEPS ETUs, over 8,000 h of development testing was completed on the 12-kW Hall thruster [8]. The successful completion of this development campaign reduced the risk of AEPS design compliance with thruster requirements and enabled AEPS to successfully complete its Critical Design Review (CDR) in March 2022 [9].

Since CDR, AR has completed assembly of one AEPS Qualification Model (QM-1) thruster and three Flight Model (FM-1, FM-2, and FM-3) thrusters. QM-1, FM-1, and FM-2 are all shown in Fig. 1. One additional Qualification Model thruster (QM-2) is in work and scheduled for completion before the end of 2025.

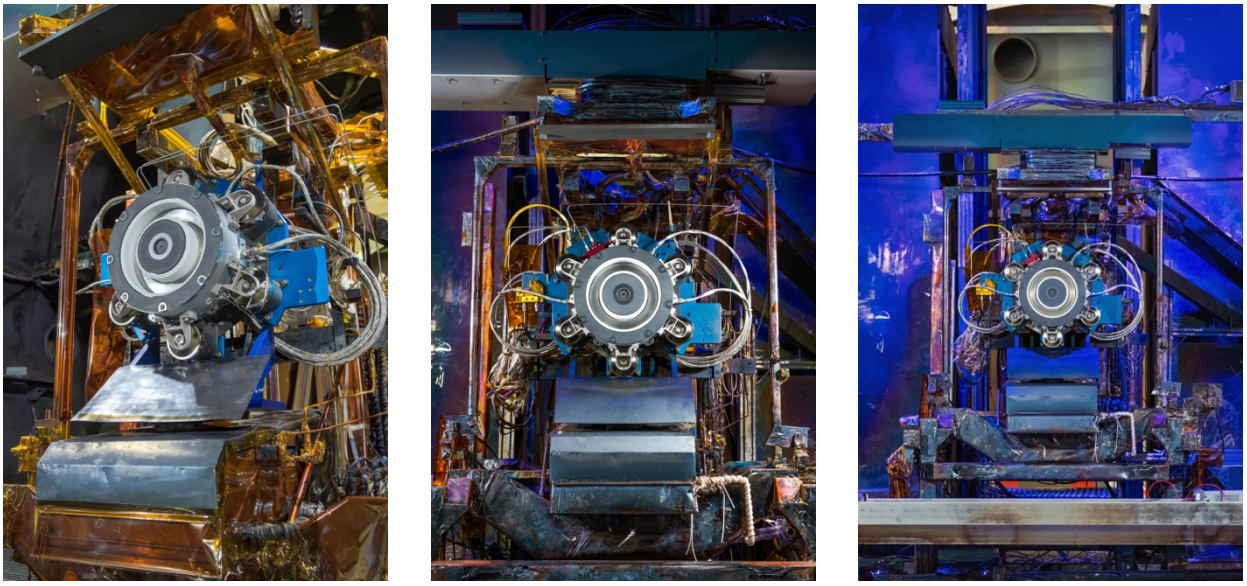

(a) **(b)** **(c)**

Fig. 1 AEPS thrusters during acceptance testing: (a) QM-1, (b) FM-1, and (c) FM-2.

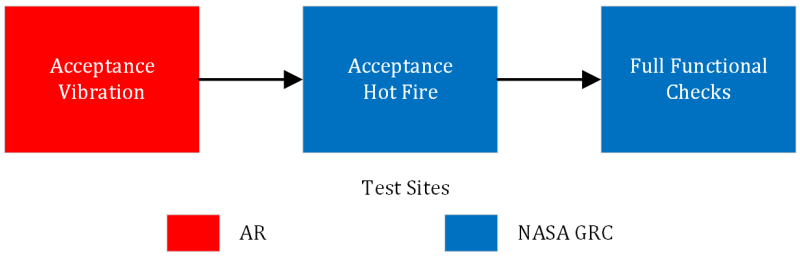

Fig. 2 AEPS FM ATP Test Flow.

Following assembly completion, all AEPS thrusters are subject to the same acceptance test program (ATP) intended to ensure that each unit is built to design, meets standards of workmanship, and is screened for build defects. The AEPS ATP sequence is shown in Fig. 2 and consists of acceptance vibration performed at AR, acceptance hot fire performed at NASA GRC, and a final set of functional tests and inspections performed at either AR (QM-1) or NASA GRC (FMs and QM-2). All test phases are a collaborative effort led by AR and executed to their test plans and procedures with NASA support. This work will present the results obtained from the ATP test sequences performed on the three AEPS units that have completed acceptance testing to date (i.e., QM-1, FM-1, and FM-2).

II. Acceptance Vibration

The AEPS ATP vibration sequence is shown in Fig. 3 with an example of the test setup shown in Fig. 4. The sequence begins with a detailed set of visual and photographic inspections followed by the performance of random and sinusoidal vibration to acceptance levels. A low-level sinusoidal sweep is performed before and after both random and sinusoidal vibration to detect any changes in thruster structural characteristics after exposure to acceptance-level mechanical environments. This sequence is repeated for all 3 thruster axes (i.e., axial and the two orthogonal axes of the exit plane). QM-1, FM-1, and FM-2 all successfully completed ATP vibration and proceeded into hot fire at GRC.

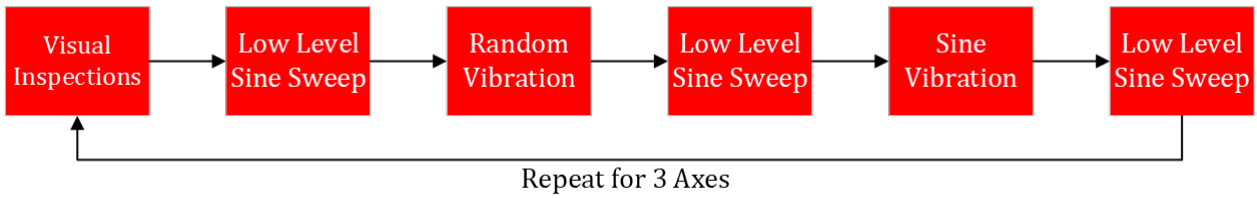

Fig. 3 AEPS acceptance vibration test sequence.

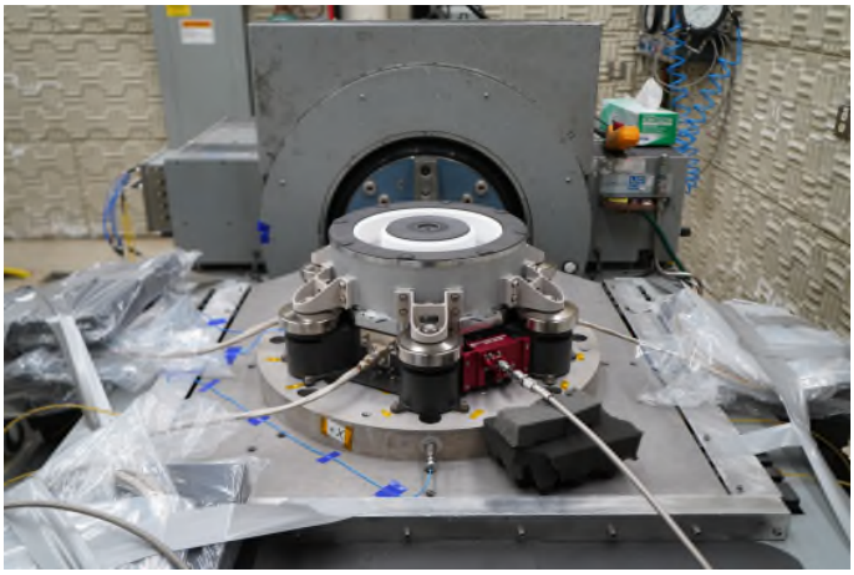

Fig. 4 AEPS FM-1 during acceptance vibration testing.

III. Acceptance Hot Fire

A. Test Sequence

The AEPS ATP hot fire test sequence is shown in Fig. 5. The sequence begins with shipment of each thruster to GRC, installation into the test facility, and detailed functional checkouts of the thruster and all ground support equipment. Following facility evacuation and initial conditioning of the magnets, cathode, and thruster, each unit undergoes an acceptance thermal cycle followed by a series of reference firings to assess performance and stability against requirements for the following four discharge powers: 9 kW, 10 kW, 11 kW, and 12 kW. Note that all throttle conditions are at a discharge voltage of 600 V.

Fig. 5 AEPS acceptance hot fire test sequence.

B. Facility and Ground Support Equipment

1. Vacuum Facility 5

All AEPS ATP hot fire sequences detailed in this work were performed in Vacuum Facility 5 (VF-5) at NASA GRC. VF-5 is a cylindrical chamber measuring 4.6 m in diameter and 18.3 m in length [10]. For these tests, VF-5 was evacuated using a series of cryopumps. The cryopumps have a combined nominal pumping speed of approximately 700,000 l/s on xenon [10–12]. In order to obtain the lowest possible background pressure, the thruster is installed in the main volume of VF-5 at the same location previously used during ETU and TDU testing [13,14]. The placement of the cryopumps relative to the thruster at this location as well as the resultant near-field background neutral distribution are described in previous work [10–12]. AEPS thrusters installed and operating in VF-5 during ATP hot fire are shown in Fig. 6 and Fig. 7, respectively.

Facility pressure was monitored with two xenon-calibrated and one nitrogen-calibrated Bayard-Alpert style hot-cathode ionization gauges. The nitrogen-calibrated gauge (SIG 2 N_2) was located approximately 0.05 m upstream of the HCT exit plane and 0.7 m below and 0.7 m radially outward from the HCT centerline; the orifice of SIG 2 N_2 faced radially outward (i.e., away from the HCT). One xenon-calibrated gauge (SIG 3 Xe) was centered approximately 0.08 m

upstream of the HCT exit plane and 0.7 m radially outward and 0.6 m below the HCT centerline; the orifice of SIG 3 Xe faced radially outward. The second xenon-calibrated gauge (SIG 2 Xe) was mounted approximately adjacent to and downstream of SIG 3 Xe and had a downstream-facing orifice.

All ion gauges used in this work were configured for operation with electric propulsion systems and thus had an elbow and plasma screen installed on the inlet of the gauge [15]. The housing of each gauge was also attached to facility ground via an electrical grounding strap to avoid charging effects and then insulated with dielectric sheeting. A thermocouple was installed on the exterior of each ion gauge tube; this allowed the measured pressures to be corrected for thermal effects [16]. The gauge temperatures and pressures were sampled using the same multiplexed DAQ used to record thruster telemetry [15]. Consistent with previous tests performed in VF-5, all pressures reported in this work correspond to the measurements made using the radially facing xenon-calibrated gauge (i.e., SIG 3 Xe) [13,14,17–20]. The average facility operating pressure during this work was approximately 4 μTorr-Xe at a total input flow rate of approximately 22 mg/s, which matches the pressures observed during previous TDU and ETU tests [21,22].

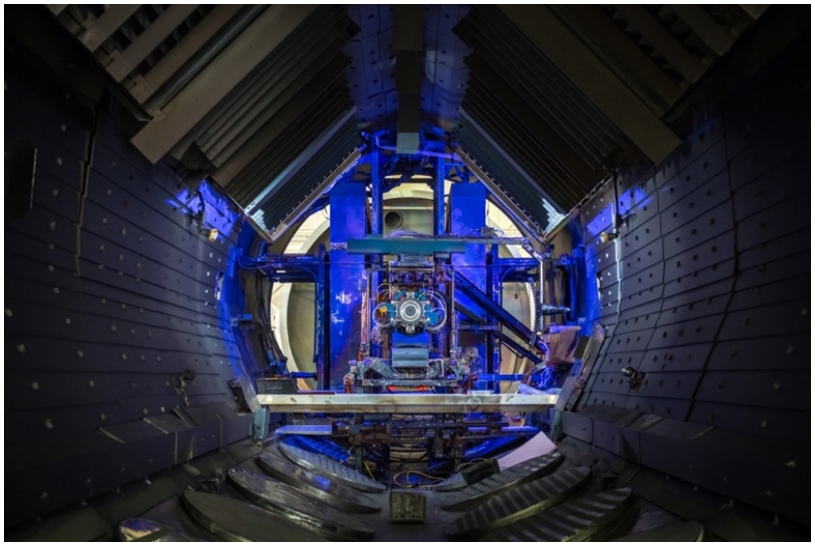

Fig. 6 AEPS FM-1 installed in VF-5 at NASA GRC.

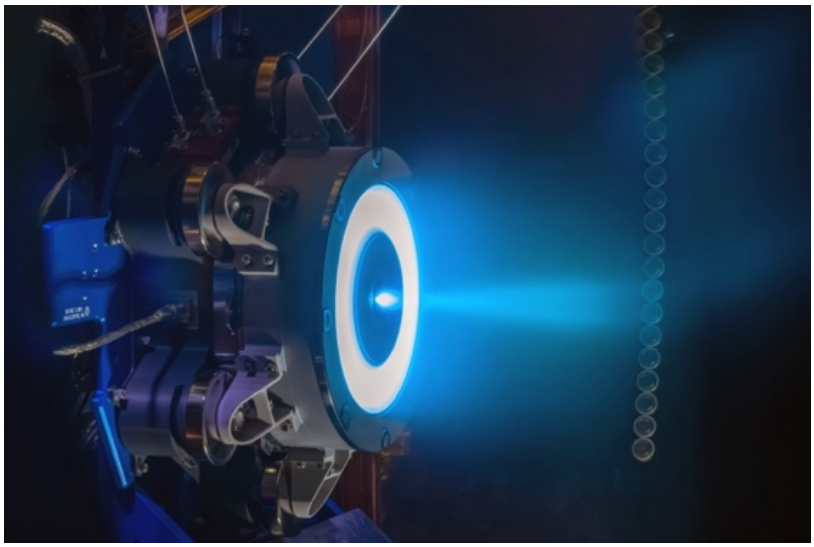

Fig. 7 AEPS QM-1 during acceptance hot fire.

2. Thruster Support Equipment

Xenon propellant was supplied to all thrusters using a laboratory feed system composed of electropolished stainless-steel lines metered with commercial thermal mass flow controllers. The anode line was metered using a 500-sccm controller, and the cathode line was metered using a 100-sccm controller. All controllers were calibrated using a piston prover with National Institute of Standards and Technology (NIST)-traceable calibrations [23]. The controllers have an uncertainty of approximately 1% of the reading for the anode and 0.35% of full-scale for the cathode. This system is identical to that used in previous TDU and ETU tests [13,14,21,24].

All thruster power was provided using a power console composed of commercial laboratory power supplies. The discharge was controlled using two 15-kW (1000 V, 15 A) power supplies connected in a controller-supporter configuration. This console is equipped with a set of safety interlocks that allows the data acquisition or vacuum facility control system to disable power and place the thruster in a safe state if a facility or thruster anomaly is detected. This setup is unchanged from previous TDU and ETU characterization and wear tests [13,14,17–21,24].

Following the results from the electrical configuration study performed by Peterson *et al.* [20], the bodies of all thrusters were electrically tied to the cathode, and all conductive surfaces within approximately one meter of the thruster exit plane were insulated using dielectric sheeting [20,25]. This was done in order to provide better control over the number of electrical coupling paths between the thruster and facility in the near-field [20,25].

Thruster telemetry was recorded continuously at a rate of approximately 8 Hz using a multiplexed data acquisition system. End-to-end calibrations of the laboratory power and data acquisition systems (DAQ) were performed using a NIST-traceable digital multimeter. The resultant uncertainty was approximately 0.03% and 0.3% of the reading for measurements of voltage and current, respectively. Voltage telemetry was measured via sense lines at the interface between the thrusters and the facility cable harness while current telemetry was measured via a set of precision shunts located in a breakout box on the air side of the thruster power feedthrough.

Waveforms of the discharge current and voltage were acquired throughout the hot fire campaign using a commercial oscilloscope equipped with 150-A AC/DC probes for current measurement and high-voltage differential probes for voltage measurements. Collected waveforms were analyzed using configuration-controlled scripts to compute the root-mean-square (RMS) and peak-to-peak (Pk-Pk) of each recorded signal.

3. Thrust Stand

Thrust was measured using the same null-type inverted pendulum thrust stand used in previous HERMeS TDU and AEPS ETU performance characterization and wear tests [13,14,17–20]. The design and theory of operation of the thrust stand are detailed in several previous works [26–28].

For all thrusters, the thrust stand was operated in a null-coil configuration. In this configuration, the position of the thruster is measured by a linear variable differential transformer (LVDT) and maintained by a pair of electromagnetic actuators. The current through each actuator is controlled using a proportional-integral-differential controller that uses the LVDT signal as the input and then modulates the current through the actuators to hold the thruster stationary. The thrust is then correlated to the resultant current through one of these actuators (i.e., the null coil). The thrust stand is also equipped with a closed-loop inclination control circuit, which uses an integral controller and piezoelectric actuator to maintain the inclination measured by an electrolytic tilt sensor and thus minimize thermal drift during performance measurements.

The thrust stand was calibrated before each set of performance measurements by loading and offloading a set of known weights using an in-situ pulley system. All reported thrust measurements have been corrected for thermal drift and offsets from the desired discharge power. The resultant thrust stand uncertainty for this work was approximately ± 5 mN [29].

C. Hot Fire Results

1. Performance

The thrust and specific impulse measured during the ATP reference fires of QM-1, FM-1, and FM-2 are shown for the 9 kW, 10 kW, 11 kW, and 12 kW operating conditions in Table 1. All measurements were acquired over a 30-minute dwell preceded by a minimum 1-h warm-up firing to limit thermal drift of the thrust stand. As shown in Table 1, no statistically significant variation in unit-to-unit performance was measured as all changes were less than the measurement uncertainty for all operating conditions.

Table 1 ATP performance results for QM-1, FM-1, and FM-2.

Discharge Power (kW)	Unit	Thrust (mN)	Specific Impulse (s)
9	QM-1	444	2610
	FM-1	446	2590
	FM-2	446	2610
10	QM-1	491	2650
	FM-1	494	2650
	FM-2	494	2670
11	QM-1	540	2700
	FM-1	542	2690
	FM-2	542	2710
12	QM-1	586	2740
	FM-1	589	2740
	FM-2	589	2750
Uncertainty		± 5	± 31

2. Oscillations

The RMS of the discharge current (I_D) as well as the peak-to-peak of the discharge current and voltage (V_D) measured during the ATP reference fires of QM-1, FM-1, and FM-2 are shown for the 9 kW, 10 kW, 11 kW, and 12 kW operating conditions in Table 2. As with the performance measurements shown in Table 1, the unit-to-unit variation in oscillation properties is less than the observed random variation from repeated measurements acquired on a single unit for all parameters and operating conditions; this indicates that no statistically significant variation in oscillation properties were observed between QM-1, FM-1, and FM-2.

Table 2 ATP oscillation results for QM-1, FM-1, and FM-2.

Discharge Power (kW)	Unit	$I_{D,\,Pk\text{-}Pk}$ (A)	$I_{D,\,RMS}$ (A)	$V_{D,\,Pk\text{-}Pk}$ (V)
9	QM-1	12.8	3.5	32
	FM-1	12.7	3.4	28
	FM-2	13.1	3.5	30
10	QM-1	12.8	3.7	31
	FM-1	13.2	3.7	29
	FM-2	13.0	3.7	30
11	QM-1	13.6	4.0	30
	FM-1	14.1	3.9	29
	FM-2	14.0	3.9	30
12	QM-1	15.2	4.2	31
	FM-1	14.9	4.1	31
	FM-2	14.7	4.2	31

IV. Full Functional Checks

Following the ATP hot fire sequence, each AEPS thruster undergoes the sequence of full functional checks shown in Fig. 8. This sequence begins with detailed post-test visual and photographic inspections. These inspections are followed by a full set of electrical (e.g., continuity, isolation, etc.) and magnetic field measurements to verify the health and state of the thruster following operation. The mass and key dimensional parameters of each thruster are then measured to verify

compliance with the AEPS interface specification. This sequence then concludes with a final set of visual and photographic inspections followed by final packaging for delivery to the end user (FMs) or next test sequence (QMs). An example of these inspections is shown in Fig. 9. AEPS QM-1, FM-1, and FM-2 each completed this sequence without incident.

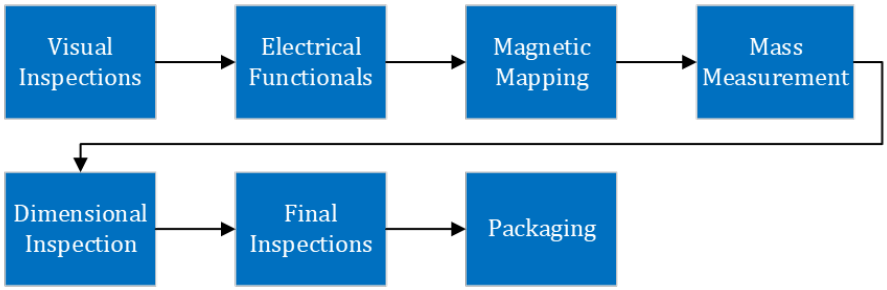

Fig. 8 Sequence of AEPS ATP full functional checks.

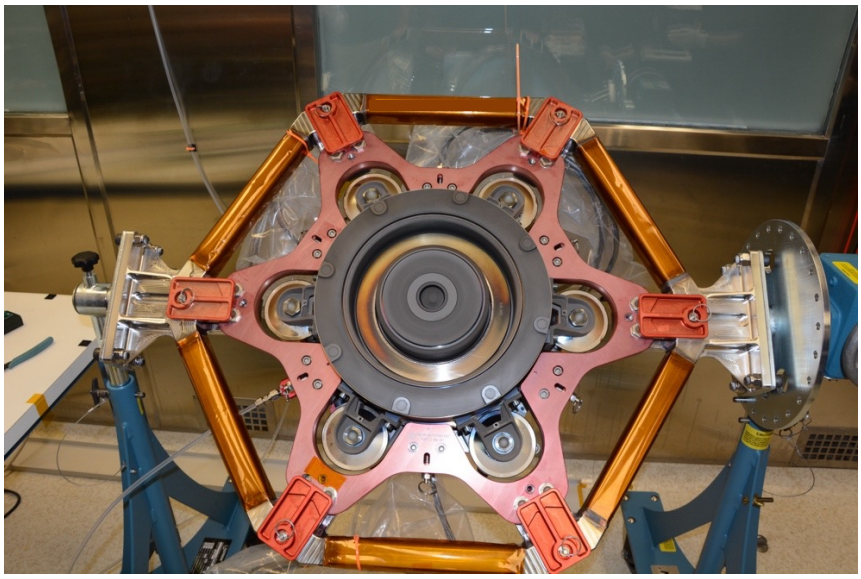

Fig. 9 AEPS FM-1 during final inspections.

V. Conclusion

This work presents an overview of the AEPS acceptance test program. The goal of this test program is to ensure that each unit is built to design, meets standards of workmanship, and is screened for build defects. The ATP consists of a vibration performed at acceptance levels, a hot fire sequence, and a final set of functional tests and inspections to verify compliance with interface requirements.

In addition to providing an overview of the test sequence, this work also summarizes the results obtained from the acceptance testing of the three qualification/flight AEPS thrusters completed to date: QM-1, FM-1, and FM-2. No statistically significant unit-to-unit variation was measured, and all three units successfully completed acceptance testing. As of writing, acceptance testing of the two remaining AEPS units (i.e., FM-3 and QM-2) are either in progress or planned for the near future.

References

[1] Congress, *National Aeronautics and Space Administration Transition Authorization Act of 2017*. 2017.
[2] Foust, J., "NASA Refines Plans for Launching Gateway and Other Artemis Elements," *SpaceNews*, 2020.
[3] Inclan, B., Anderson, G., and Russell, J., "NASA Awards Artemis Contract for Lunar Gateway Power, Propulsion," NASA, Release 19-042, 2019.
[4] Herman, D. A., Gray, T., Johnson, I., Kerl, T., Lee, T., and Silva, T., "The Application of an Advanced Electric Propulsion System on the NASA Power and Propulsion Element (PPE)," *36th International Electric Propulsion Conference*, Electric Rocket Propulsion Society, IEPC Paper 2019-651, Fairview Park, OH, 2019.
[5] Ticker, R., Gates, M., Manzella, D., Biaggi-Labiosa, A., and Lee, T., "The Gateway Power and Propulsion Element: Setting the Foundation for Exploration and Commerce," *2019 Propulsion and Energy Forum*, American Institute of Aeronautics and Astronautics, AIAA Paper 2019-3811, Reston, VA, 2019.
[6] Jackson, J., Miller, S., Cassady, J., Soendker, E., Welander, B., Barber, M., and Peterson, P. Y., "13 kW Advanced Electric Propulsion Flight System Development and Qualification," *36th International Electric Propulsion Conference*, Electric Rocket Propulsion Society, IEPC Paper 2019-692, Fairview Park, OH, 2019.
[7] Frieman, J. D., Kamhawi, H., Mackey, J., Peterson, P. Y., Gilland, J. H., Hofer, R. R., Inaba, D., Dao, H., Branch, N. A., and Welander, B., "Extended Wear Testing of the 12-kW Advanced Electric Propulsion System Engineering Test Unit Hall Thruster," *37th International Electric Propulsion Conference,* Electric Rocket Propulsion Society, IEPC Paper 2022-362, Fairview Park, OH, 2022.
[8] Frieman, J. D., Kamhawi, H., Mackey, J., Soulas, G., Peterson, P. Y., and Gilland, J. H., "Edge Wear of the Advanced Electric Propulsion System Pole Covers," AIAA SCITECH 2023 Forum, American Institute of Aeronautics and Astronautics, AIAA Paper 2023-1024, 2023.
[9] Shastry, R., Kamhawi, H., Frieman, J. D., Soulas, G. C., Gray, T. G., Verhey, T. R., Kachele, C. D., Williams, G. J., Fisher, J., Blackner, G., Forbes, E., Hondagneu, J., Branch, N. A., and Watts, H., "12-kW Advanced Electric Propulsion System Hall Current Thruster Qualification and Production Status," *38th International Electric Propulsion Conference,* Electric Rocket Propulsion Society, IEPC Paper 2024-298, 2024.
[10] Lobo, M. J., "Electric Propulsion Laboratory | NASA Glenn Research Center," 2017.
[11] Yim, J. and Burt, J. M., "Characterization of Vacuum Facility Background Gas Through Simulation and Considerations for Electric Propulsion Ground Testing," *51st AIAA/SAE/ASEE Joint Propulsion Conference*, American Institute of Aeronautics and Astronautics, AIAA Paper 2015-3825, Reston, VA, 2015.
[12] Yim, J. T., Herman, D. A., and Burt, J. M., "Modeling Analysis for NASA GRC Vacuum Facility 5 Upgrade," NASA Glenn Research Center, Cleveland, OH, NASA/TM 2013-216496, 2013.
[13] Williams, G. J., Kamhawi, H., Choi, M., Haag, T., Huang, W., Herman, D. A., Gilland, J. H., *et al.*, "Wear Trends of the HERMeS Thruster as a Function of Throttle Point," *35th International Electric Propulsion Conference*, Electric Rocket Propulsion Society, IEPC Paper 2017-207, Fairview Park, OH, 2017.
[14] Williams, G., Gilland, J. H., Peterson, P. Y., Kamhawi, H., Huang, W., Swiatek, M., Joppeck, C., *et al.*, "2000-hour Wear Testing of the HERMeS Thruster," *52nd AIAA/SAE/ASEE Joint Propulsion Conference*, American Institute of Aeronautics and Astronautics, AIAA Paper 2016-5025, Reston, VA, 2016.
[15] Dankanich, J. W., Walker, M., Swiatek, M. W., and Yim, J. T., "Recommended Practice for Pressure Measurement and Calculation of Effective Pumping Speed in Electric Propulsion Testing," *Journal of Propulsion and Power*, Vol. 33, No. 3, 2017, pp. 668–680.
[16] "Standard Practice for Ionization Gage Application to Space Simulators," ASTM International, West Conshohocken, PA, E296-70, 2015.
[17] Kamhawi, H., Huang, W., Gilland, J., Haag, T., Mackey, J., Yim, J., Pinero, L., Williams, G., Peterson, P., and Herman, D., "Performance, Stability, and Plume Characterization of the HERMeS Thruster with Boron Nitride Silica Composite Discharge Channel," Fairview Park, OH, 2017.
[18] Kamhawi, H., Huang, W., Haag, T., Yim, J., Herman, D., Peterson, P. Y., Williams, G., *et al.*, "Performance, Facility Pressure Effects, and Stability Characterization Tests of NASA's Hall Effect Rocket with Magnetic Shielding Thruster," *52nd AIAA/SAE/ASEE Joint Propulsion Conference*, American Institute of Aeronautics and Astronautics, AIAA Paper 2016-4826, Reston, VA, 2016.
[19] Huang, W., Kamhawi, H., and Haag, T., "Facility Effect Characterization Test of NASA's HERMeS Hall

Thruster," *52nd AIAA/SAE/ASEE Joint Propulsion Conference*, American Institute of Aeronautics and Astronautics, AIAA Paper 2016-4828, Reston, VA, 2016.
[20] Peterson, P. Y., Kamhawi, H., Huang, W., Williams, G., Gilland, J. H., Yim, J., Hofer, R. R., *et al.*, "NASA's HERMeS Hall Thruster Electrical Configuration Characterization," *52nd AIAA/SAE/ASEE Joint Propulsion Conference*, American Institute of Aeronautics and Astronautics, AIAA Paper 2016-5027, Reston, VA, 2016.
[21] Frieman, J. D., Kamhawi, H., Mackey, J., Haag, T. W., Peterson, P. Y., Herman, D. A., Gilland, J. H., *et al.*, "Completion of the Long Duration Wear Test of the NASA HERMeS Hall Thruster," *2019 Joint Propulsion Conference*, American Institute of Aeronautics and Astronautics, AIAA Paper 2019-3895, Reston, VA, 2019.
[22] Frieman, J. D., Kamhawi, H., Huang, W., Mackey, J. A., Ahern, D. M., Peterson, P. Y., Gilland, J., *et al.*, "Wear Test of the 12.5-kW Advanced Electric Propulsion System Engineering Test Unit Hall Thruster," *2020 Propulsion and Energy Forum*, American Institute of Aeronautics and Astronautics, AIAA Paper 2020-3625, Reston, VA, 2020.
[23] Padden, H., "Ultra Low Flow Fast Primary Gas Prover," presented at the Measurement Science Conference, Butler, NJ, Bios International Corporation, Butler, NJ, 2009.
[24] Frieman, J. D., Kamhawi, H., Williams, G. J., Huang, W., Herman, D. A., Peterson, P. Y., Gilland, J. H., *et al.*, "Long Duration Wear Test of the NASA HERMeS Hall Thruster," *2018 Joint Propulsion Conference*, American Institute of Aeronautics and Astronautics, AIAA Paper 2018-4645, Reston, VA, 2018.
[25] Frieman, J. D., King, S. T., Walker, M. L. R., Khayms, V., and King, D., "Role of a Conducting Vacuum Chamber in the Hall Effect Thruster Electrical Circuit," *Journal of Propulsion and Power*, Vol. 30, No. 6, 2014, pp. 1471–1479.
[26] Xu, K. G. and Walker, M. L. R., "High-power, Null-type, Inverted Pendulum Thrust Stand," *Review of Scientific Instruments*, Vol. 80, No. 5, 2009, pp. 55103–55103.
[27] Haag, T. W., "Thrust Stand for High-power Electric Propulsion Devices," *Review of Scientific Instruments*, Vol 62, No. 5, 1991, pp. 1186–1191.
[28] Polk, J.E., Pancotti, A., Haag, T., King, S., and Walker, M., "Recommended Practices in Thrust Measurements," *33rd International Electric Propulsion Conference*, Electric Rocket Propulsion Society, IEPC Paper 2013-440, Fairview Park, OH, 2013.
[29] Mackey, J., Haag, T. W., Kamhawi, H., Hall, S. J., and Peterson, P. Y., "Uncertainty in Inverted Pendulum Thrust Measurements," *54th AIAA/SAE/ASEE Joint Propulsion Conference*, American Institute of Aeronautics and Astronautics, AAA Paper 2018-4516, Reston, VA, 2018.